Structural and mechanistic studies of chloride induced activation of human pancreatic α-amylase

ROBERT MAURUS,[1] ANJUMAN BEGUM,[1] HSIN-HEN KUO,[1] ANDREW RACAZA,[1] SHIN NUMAO,[2] CARSTEN ANDERSEN,[4] JEPPE W. TAMS,[4] JESPER VIND,[4] CHRISTOPHER M. OVERALL,[1,3] STEPHEN G. WITHERS,[1,2] AND GARY D. BRAYER[1]

[1]Department of Biochemistry and Molecular Biology, [2]Department of Chemistry, and [3]Department of Oral Biological and Medical Sciences, University of British Columbia, Vancouver, British Columbia, Canada
[4]Novozymes, DK-2880 Bagsvaerd, Denmark

(RECEIVED August 28, 2004; FINAL REVISION November 3, 2004; ACCEPTED November 4, 2004)

Abstract

The mechanism of allosteric activation of α-amylase by chloride has been studied through structural and kinetic experiments focusing on the chloride-dependent N298S variant of human pancreatic α-amylase (HPA) and a chloride-independent TAKA-amylase. Kinetic analysis of the HPA variant clearly demonstrates the pronounced activating effect of chloride ion binding on reaction rates and its effect on the pH-dependence of catalysis. Structural alterations observed in the N298S variant upon chloride ion binding suggest that the chloride ion plays a variety of roles that serve to promote catalysis. One of these is having a strong influence on the positioning of the acid/base catalyst residue E233. Absence of chloride ion results in multiple conformations for this residue and unexpected enzymatic products. Chloride ion and N298 also appear to stabilize a helical region of polypeptide chain from which projects the flexible substrate binding loop unique to chloride-dependent α-amylases. This structural feature also serves to properly orient the catalytically essential residue D300. Comparative analyses show that the chloride-independent α-amylases compensate for the absence of bound chloride by substituting a hydrophobic core, altering the manner in which substrate interactions are made and shifting the placement of N298. These evolutionary differences presumably arise in response to alternative operating environments or the advantage gained in a particular product profile. Attempts to engineer chloride-dependence into the chloride-independent TAKA-amylase point out the complexity of this system, and the fact that a multitude of factors play a role in binding chloride ion in the chloride-dependent α-amylases.

Keywords: amylase; chloride activation; catalytic activity; acarbose; inhibition; active site; kinetics; X-ray crystallography; protein folding

α-Amylase (α-1,4 glucan-4-glucanohydrolase, EC 3.2.1.1) is an endoglycosidase, which hydrolyses starch and related α-1,4–linked glycosyl polysaccharides. Although found in many organisms, the primary sequences of α-amylases show poor sequence homology. In contrast, the three-dimensional structures of these enzymes are found to be remarkably conserved in organisms ranging from microbial to mammalian (Boel et al. 1990; Kadziola et al. 1994; Brayer et al. 1995; Machius et al. 1995; Ramasubbu et al. 1996; Brzozowski and Davies 1997). Prominent among the structural similarities observed are the common presence of three domains. Domain A consists of an α/β barrel and contains the active site; domain B protrudes from the side of domain A and contains the calcium binding site; and domain C forms a structurally independent antiparallel β-barrel. The corresponding structural features of human pancreatic α-amylase (HPA) are illustrated in Figure 1.

Significant progress has been made in elucidating the catalytic mechanism of this family of enzymes (Tao et al.

Reprint requests to: Gary D. Brayer, Department of Biochemistry and Molecular Biology, University of British Columbia, Vancouver, BC, Canada V6T 1Z3; e-mail: brayer@interchange.ubc.ca; fax: (604) 822-5227.

Abbreviations: HPA, human pancreatic α-amylase; CNP-G3, 2-chloro-4-nitrophenyl-α-maltotrioside; TAKA-amylase, *Aspergillus orzyae* α-amylase; Ani3038, variant Taka-amylase protein containing the mutations W61Q, L250T, and I326R (TAKA-amylase numbering) that was created for this study. Amino acid numbering is according to the sequence alignment presented in Brayer et al. 1995 unless otherwise noted.

Article and publication are at http://www.proteinscience.org/cgi/doi/10.1110/ps.041079305.

1989; Braun et al. 1995; Rydberg et al. 1999; Uitdehaag et al. 1999). Overall, α-amylases, which are retaining glycosidases, catalyze substrate hydrolysis by a double displacement mechanism whereby a covalent glycosyl-enzyme intermediate is formed and hydrolyzed through oxocarbenium ion-like transition states (Zechel and Withers 2000; Vasella et al. 2002). A required feature of this mechanism is the presence of two carboxylic acid-containing side chains in the active site of the enzyme. One of these carboxylic acids (D197 in HPA) acts as the catalytic nucleophile and displaces the aglycon portion of the substrate upon formation of the covalent intermediate. The other carboxylic acid acts as the acid/base catalyst (E233 in HPA) and thereby assists in the stabilization of the two transition states proposed to occur in the hydrolysis process (see Fig. 2 of Brayer et al. 2000).

Interestingly, some members of this family of enzymes, including human pancreatic α-amylase (HPA), are allosterically activated by chloride (D'Amico et al. 2000). Chloride binding has been found to modulate both the maximal activity and pH optima of such enzymes (Wakim et al. 1969; Steer and Levitzki 1973; Levitzki and Steer 1974; Feller et al. 1996; Aghajari et al. 2002; Numao et al. 2002). The conserved chloride ion binding site in the chloride-dependent amylases is constituted from an arginine, an asparagine, and another basic residue. This positions the chloride ion in close proximity to the active site residues (~5 Å) and the substrate binding cleft. This placement of chloride ion and the observed dependence of enzymatic activity on this moiety, clearly suggests that chloride ion binding is designed to modulate the properties of active site residues to facilitate catalytic activity.

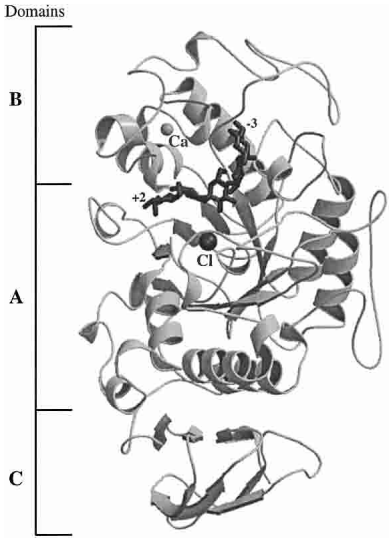

Figure 1. A ribbon diagram showing the overall structure of human pancreatic α-amylase, which is folded into three domains (*A*–*C*). The positions of bound chloride (a catalytic activator) and calcium (a structural stabilizer) are also indicated with large spheres, along with the bound conformation of the inhibitor product produced when acarbose is bound in the active site (subsites −3 and +2 are labeled).

High-resolution studies have delineated the structural determinants and detailed interactions that form the chloride ion binding site in HPA (Brayer et al. 1995; Numao et al. 2002). The three residues that play a direct role in binding chloride ion include R195, N298, and R337. Notably, the side chain of R195 is also directly hydrogen bonded to the side chain of D197, this latter residue being the catalytic nucleophile (Rydberg et al. 1999), as well as to the side chain of E233, a prime candidate to function as the acid/base catalyst. Also, R195 along with H299 and D300, form hydrogen bonds to the substrate glucose ring bound in the −1 binding subsite. It is this glucose moiety that is attacked by the catalytic nucleophile during enzymatic hydrolysis (Brayer et al. 2000). Somewhat further removed from the active site is the N298 ligand of bound chloride. The side chain of this residue also binds to a water molecule that may play the role of nucleophile in the cleavage of the covalent intermediate formed during catalysis. The third chloride binding ligand is R337, which is more remotely located at the bottom of the chloride ion-binding pocket.

In previous studies of human pancreatic α-amylase, we have carefully examined the roles of the positively charged chloride ligands R195 and R337, through a structure–function–mutagenesis approach (Numao et al. 2002). For the series of substitutions R195A, R195Q, R337A, and R337Q, no chloride binding could be detected in variant enzymes, and crystallographic analysis confirmed this finding while also showing that the structure was not perturbed. However, these variant proteins did have different kinetic properties. The most pronounced differences involved the R195 variants, with activities 20–450-fold lower than wild-type and pH optima shifted to a more basic pH. More modest kinetic changes were observed for the R337 variants (twofold) and interestingly, neither variant was chloride-dependent. In related work with *Pseudoalteromonas haloplantis* α-amylase, replacement of the equivalent chloride ion ligand to R337 produced similar results, although with a somewhat larger decrease in catalytic activity (eight times less for the K300Q variant) (Aghajari et al. 2002). Collectively, these results demonstrate that R337 and R195 are both involved in the binding of chloride ion. However, as the decrease in catalytic activity indicates, R195 also plays a key role in transition state stabilization.

An essential missing element to more comprehensively understanding the mechanistic aspects of chloride activation in enzymes like HPA has been the inability to simultaneously study the functional and structural attributes of such enzymes in both the presence and absence of chloride ion, and additionally with and without bound substrates or inhibitors. While it would be best to study wild-type HPA in this manner, its relatively high affinity for chloride ion and the requirements of crystallization conditions necessary for

structural studies has blocked progress in this area. Another approach to overcome this problem is to examine a variant structure that has a significantly reduced, but not abolished, affinity for chloride ion. In an earlier study, we have detected and preliminarily characterized one such variant, N298S (Numao et al. 2002). This variant protein has a chloride dissociation constant of 162 mM (compared to 0.52 mM for wild-type HPA), nicely in a range that facilitates both kinetic and structural analyses. It has the further advantage of allowing for the characterization of the properties of the third major ligand to bound chloride ion, N298. While completely conserved in α-amylase primary sequences, and apparently a major determinant in both chloride binding and the placement of the active site residue D300, the role of N298 has not been studied in detail. Herein, we report a comprehensive analysis of the role of this residue, and structural and kinetic analyses of the N298S variant in both the presence and absence of chloride ion. It has also proven possible to examine the hydrolysis and transglycosylation activities of this variant HPA using the naturally occurring and therapeutically utilized inhibitor acarbose as a reporter molecule. We also report attempts to engineer chloride-dependence into the chloride-independent TAKA-amylase.

Results

Kinetic analyses of N298S variant HPA

Previous studies showed that, in contrast to what was seen with the other residues of the chloride ion-binding site, mutation of N298 to a serine does not remove the dependence upon chloride concentration (Numao et al. 2002). It does, however, result in a lower affinity for chloride ions (K_d = 162 mM when checked by activity of HPA against starch). The mutation also resulted in a 10-fold decrease of catalytic activity with starch. This is not completely surprising, as N298 appears to play at least two other key roles in the active site of HPA. These include anchoring a portion of polypeptide chain (residues 299–305) that is highly mobile in the resting state of the enzyme, and substantially reoriented and stabilized upon binding of substrates to the active site (Rydberg et al. 2002). Of particular importance within this loop are H299, D300, and H305, which form hydrogen bond interactions to bound substrates in the −1 and −2 binding subsites in the active site crevice. Another role that the side chain of N298 plays, in conjunction with the side chains of E233 and D300, is in coordinating a water molecule that may play a key role in the deglycosylation step. The uncertainty in the structural and functional relationship between N298 and bound chloride ion has necessitated further study.

Our previous work with starch as substrate showed that the N298S variant of HPA retained the classic dependence of rate and pH optimum upon chloride concentration. In this paper we refine and extend this kinetic analysis using the homogenous and reproducible substrate CNP-G3. At a pH of 7.0, the activities of both the wild-type HPA and N298S variant HPA on CNP-G3 were shown to be dependent on chloride concentration (Fig. 2A). Using the activity as a measure of chloride binding, the dissociation constants for the chloride ion were determined to be 0.5 mM and 93 mM for the wild-type and N298S variant of HPA, respectively. This is quite consistent with the data obtained using starch as a substrate where K_d values of 0.5 mM and 162 mM were measured.

The pH-dependence of k_{cat}/K_m with CNP-G3 substrate reflects ionizations in the free enzyme. As can be seen in Figure 2, B and C, a bell-shaped dependence is seen for both the wild-type and N298S variant HPA, and the simplest interpretation is that the two ionizations observed are associated with the catalytic nucleophile (D197-acid limb) and the acid/base catalyst (E233-basic limb). Previous studies involved starch as substrate, and reported values of k_{cat} as a function of pH, thus reflecting ionizations in the enzyme/substrate complex. In this study of ionizations in the free enzyme, in both cases (wild-type and N298S) pK_{a1} was largely independent of chloride concentration (Table 1; the increase at 600 mM could well be a salt effect), as was also seen previously for ionizations in the ES complex of wild-type enzyme. This is consistent with the fact that D197 is not located in direct proximity to the chloride site. However, pK_{a1} for the free N298S is a full 1.5 units lower than for the WT enzyme, indicating a substantial change in environment. As seen with the WT enzyme pK_{a2} is very dependent on chloride concentration, shifting almost 2 pK_a units in its presence.

N298S variant structure in the absence of chloride ion

X-ray crystallographic studies of the N298S variant of HPA performed in the absence of chloride show that the chloride ion binding site is indeed vacant. The absence of chloride ion causes little perturbation of the overall polypeptide chain fold of HPA, with the average deviation between main chain atoms of the wild-type and variant enzymes being 0.13 Å. However, removal of this chloride ion, as well as the side chain of N298, does result in substantial shifts in the positions of the side chains of both of the active site residues E233 and D300 (Figs. 3, 4A, 5). The side chain of D300 moves toward the space created by substituting the smaller side chain of serine for asparagine at residue 298. As a result of this large shift, the side chain of D300 becomes hydrogen bonded to the side chain of S298 (d = 2.5 Å) (Figs. 4A, 5).

Two new features also serve to fill the additional volume generated in the chloride ion binding site in the absence of this moiety. The first of these is a large shift in the side chain of E233 into this cavity, through rotation about the X_1 torsional angle of its side chain. This movement substan-

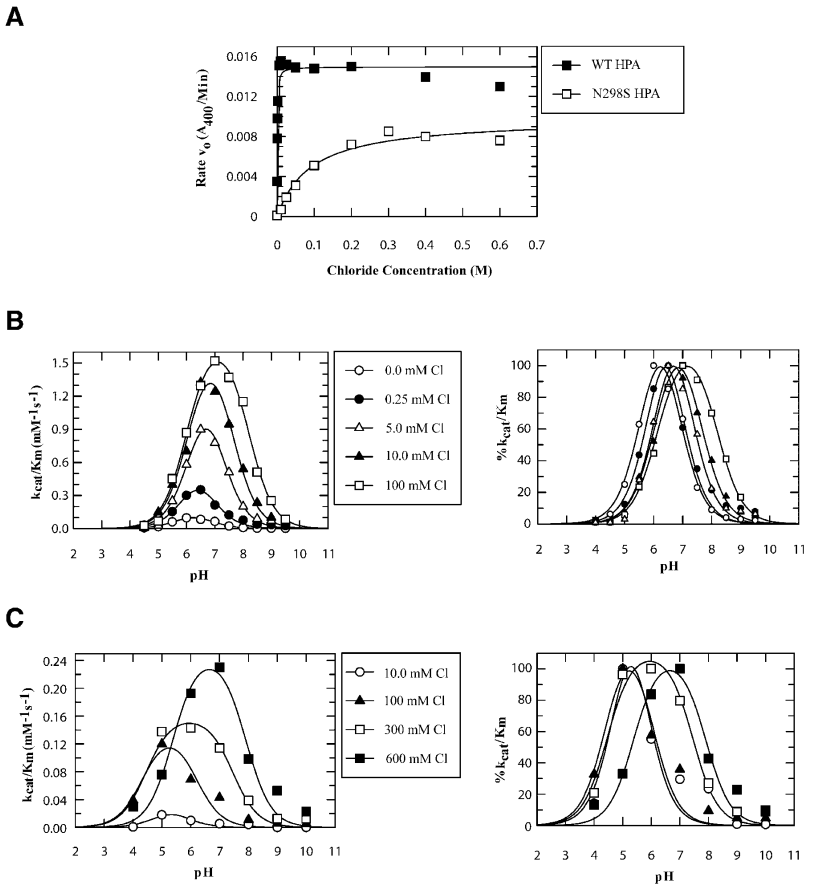

Figure 2. Kinetic results obtained for the wild-type and N298S variant of HPA using CNP-G3 as substrate. (*A*) The dependence of initial hydrolysis rates on chloride concentration is shown. (*B*) For wild-type and (*C*) for the N298S variant HPA, the pH dependence of k_{cat}/K_m on increasing chloride concentration is shown, along with the associated normalized curves.

tially changes the relative orientations of the catalytic residues of HPA, and very likely explains the large decrease in hydrolysis rates observed for the N298S variant at lower chloride concentrations (Table 1; Fig. 2). Within this modified active site, two water molecules are found at the former locations of the terminal OE oxygen atoms of the E233 side chain. In its new orientation, the extremity of the E233 side chain is located only 1.8 Å from the position of bound chloride ion in the wild-type enzyme. Here, the E233 side chain appears to form a direct salt bridge with the side chain of R337 (d = 2.9 Å), a key chloride ion ligand in the wild-type enzyme. In wild-type HPA, direct E233–R337 contact is not possible due to the positioning of the bound chloride ion. Indeed, the absence of R337 in chloride-independent amylases may well relate to the need to avoid such an interaction with E233, which would disrupt the normal orientation of catalytic residues in the active site. This would also explain the finding (Numao et al. 2002) that no structural change was observed upon substitution of R337 for glutamine, but a chloride-independent amylase was produced.

A second feature serving to fill the vacant chloride ion binding site in the N298S variant is a new, tightly bound water molecule, centrally positioned between the shifted side chains of D300 and E233, as well as the now shorter side chain of S298 (Figs. 4A, 5). Beyond hydrogen bonds to these residues, the side chains of two former chloride ion ligands, R195 and R337, are within hydrogen bonding distance. As Figure 4A shows, neither of these latter two side chains is significantly displaced in the absence of bound chloride ion. Notably, as a consequence of the relocation of the side chain of E233, this new water molecule cannot be positioned where one would normally find bound chloride ion. Instead, it is shifted 1.4 Å from this position toward the open space generated by the replacement of N298 by a serine residue.

The chloride-containing N298S HPA structure

Our structural studies show that at high chloride concentrations, a chloride ion is indeed found bound to the N298S variant of HPA at full occupancy in its binding pocket adjacent to the active site (Fig. 4A). A comparison of the structure of this variant and that of wild-type HPA reveals

Table 1. *Summary of kinetic parameters*

A. pK_a values obtained from k_{cat}/K_m versus pH dependence curves (see Fig. 2) of wild-type and N298S HPA at different chloride concentrations. The limiting value of k_{cat}/K_m was derived from the fit for each ionization curve.

	[Cl] (mM)	pK_{a1}	pK_{a2}	k_{cat}/K_m
WT	0.00	5.73	6.75	0.20
	0.25	5.97	6.82	0.80
	5.00	6.02	7.27	1.70
	10.0	6.09	7.59	1.90
	100	6.01	8.19	1.80
N298S	10.0	4.24	5.99	0.03
	100	4.35	6.18	0.15
	300	4.45	7.44	0.16
	600	5.37	7.90	0.25

B. Kinetic parameters measured for wild-type and N298S HPA using 2-chloro-4-nitrophenyl-α-maltotrioside (CNP-G3) as a substrate at pH 7.0.

	[Cl] (mM)	K_m (mM)	k_{cat} (s^{-1})	k_{cat}/K_m (mMs^{-1})	K_i (Acarbose) (μM)
WT	10	0.74	2.98	2.21	5.0
N298S	300	0.60	0.87	1.45	6.0

C. Initial rates of product formation at two different chloride concentrations and two pH values for the TAKA and Ani3038 variant amylases using CNP-G3 as a substrate. Rates were determined by an increase in absorbance at 400 nm (ΔAbs/sec).

	0 mM Cl (pH 5.0)	0 mM Cl (pH 7.0)	300 mM Cl (pH 5.0)	300 mM Cl (pH 7.0)
TAKA-amylase	2.7×10^{-4}	1.0×10^{-4}	4.5×10^{-4}	7.7×10^{-5}
Ani3038 variant	4.0×10^{-4}	1.4×10^{-4}	5.6×10^{-4}	1.0×10^{-4}

that the chloride ion positions are within 0.15 Å and their thermal factors are 22 $Å^2$ and 16 $Å^2$, respectively, suggesting that the chloride plays its activating role in the same way. Although the overall average main chain conformation of the chloride bound N298S variant is similar to that of its chloride-deficient counterpart (Δd = 0.12 Å) and wild-type HPA (Δd = 0.12 Å), the presence of chloride ion does have a marked effect on the placement of the side chains of the active site residues E233 and D300 (Figs. 4A, 5).

In the presence of the chloride ion, the side chain of E233 rotates out of the chloride ion binding pocket toward a wild-type orientation. Within its binding site, the chloride ion forms the expected interactions to R195 and R337 (Figs. 4A, 5). It is, however, too distant to form a direct hydrogen bond interaction with the shorter side chain of S298. In addition, the presence of chloride ion causes the side chain of D300 to take on a conformation similar to that found in the wild-type enzyme. Therefore, the overall placement of chloride and nearby active site residues in the N298S variant structure turns out to be very similar to that found in the wild-type enzyme, with a water molecule playing the role of the missing ND2 of the side chain amide group of N298 (Δd Wat-ND2 = 1.0 Å).

N298S variant/acarbose complexation in the presence of bound chloride

Wild-type HPA rearranges the naturally occurring inhibitor acarbose through a series of hydrolysis and transglycosylation events forming a pseudo-pentasaccharide, which is then tightly bound in the active site cleft (Brayer et al. 2000). The rearranged product spans subsites −3 to +2, with the two rings of the acarviosine group positioned in subsites −1 and +1, between which the hydrolysis of substrates would normally occur. The *N*-linked "glycosidic" bond between these two rings of acarviosine makes this group resistant to hydrolysis and the resultant complex is thought to resemble the transition state. Given the catalytic reactions undertaken and the tight binding observed for the resultant product, the mode of acarbose binding is an ideal tool for monitoring the impact of amino acid replacements on the function of HPA.

The acarbose product complex formed with the N298S variant in the presence of bound chloride ion is the same as that found for wild-type HPA (Brayer et al. 2000). This includes the full range of very extensive interactions formed in the extended binding cleft of HPA (Figs. 4B, 6) and the minor polypeptide chain shifts required to bind this inhibitor (average Δd for main chain atoms = 0.17 Å). The chloride ion is also found at nearly the same position as in wild-type HPA (Δd = 0.10 Å) (Figs. 4B, 5) and a water molecule fills the additional space available with the exchange of the side chain of N298 with serine. Overall, our observation of normal inhibitor product formation and related active site interactions suggests that the catalytic machinery of the N298S variant in the presence of chloride is active and functioning in the normal manner, albeit somewhat less efficiently (Fig. 2).

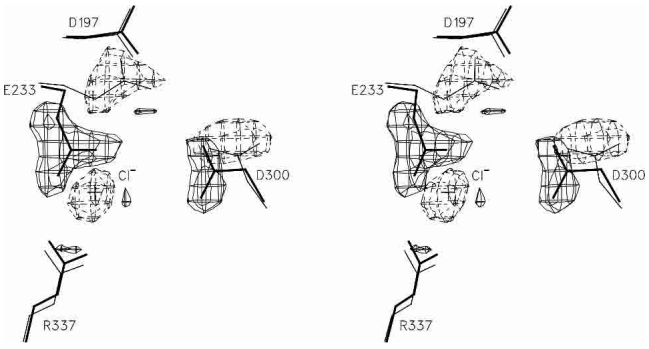

Figure 3. A stereo drawing of the Fo(N298S, chloride absent) – Fo(N298S, chloride present) difference electron density map in the vicinity of catalytic residues and the chloride ion binding site. This map is drawn at the 3.5σ level (solid lines, positive density; dashed lines, negative density). Notably in the N298S variant structure of HPA, removal of chloride ion results in the reorientation of the side chains of the catalytic residues E233 and D300 toward the vacant space generated in the chloride binding site. In this drawing, thin lines correspond to the N298S, chloride present structure, whereas thick lines indicate the N298S, chloride absent structure. As can be clearly seen, the more distantly positioned catalytic nucleophile, D197, is not significantly affected by the absence of chloride binding.

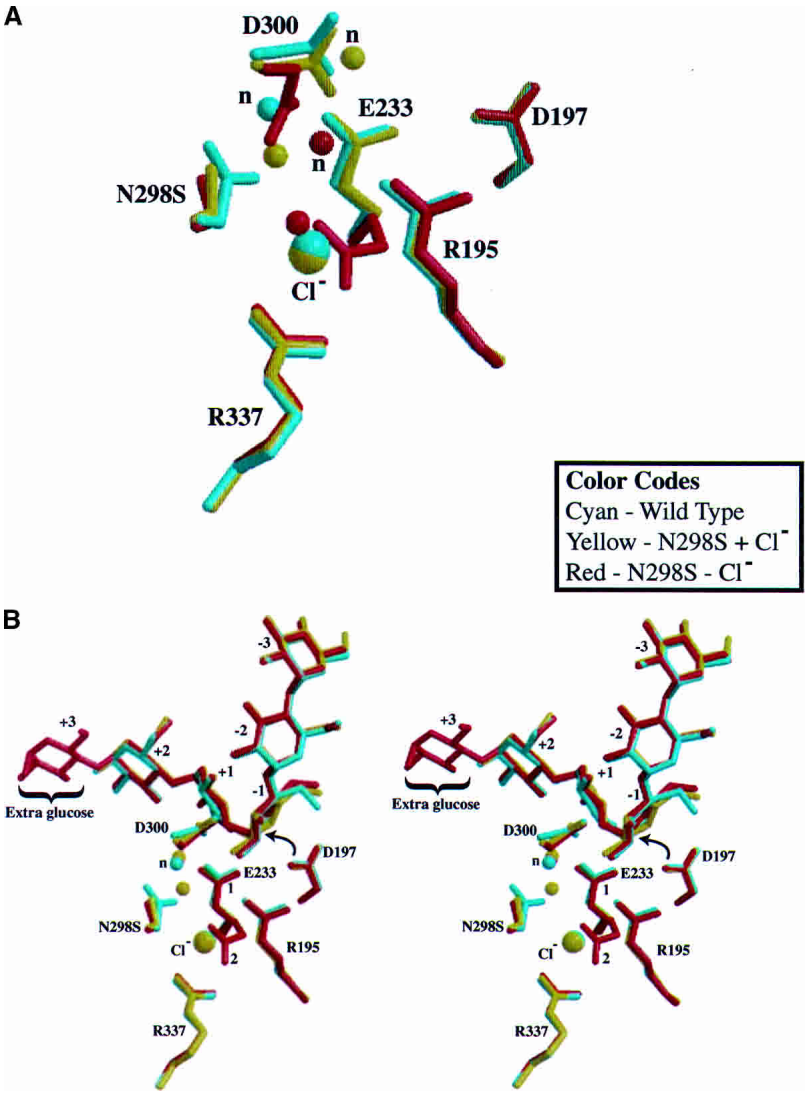

Figure 4. Color plots of the HPA chloride binding and active site regions in the N298S variant (*A*) in the absence (red) and the presence (yellow) of chloride ion, and in the wild-type enzyme (cyan), and this same region drawn as a stereo diagram (*B*) when the inhibitor acarbose is bound (color coded according to the structure involved). Notably, the side chains of both D300 and E233 are shifted toward the vacant space generated in the N298S variant when chloride ion is absent. When acarbose is bound and chloride is absent, D300 returns to its normal orientation, while E233 is found to have two conformations (labeled *1* and *2*), occupied on an approximately equal basis. Surprisingly, the final inhibitor product observed in this case is 1 sugar residue longer, and as labeled, in total spans subsites +3 to −3. In all structures, D197 maintains a comparable positioning and its mode of nucleophilic attack on the C1 carbon of the sugar ring of a normal substrate in the −1 subsite is shown with an arrow. In both diagrams, the water molecule believed to act as the nucleophile in breaking down the covalent glycosyl-enzyme intermediate formed during hydrolysis is labeled "n."

Unusual inhibitor product formation in the chloride-deficient N298S variant

A markedly different structure is observed in the acarbose product complex with the N298S variant HPA in the absence of chloride. Here, the rearranged acarbose product is a pseudo-hexasaccharide with the additional glucose ring bound in the +3 subsite (Figs. 4B, 7). This leads to not only additional protein–inhibitor interactions in this subsite, but also changes in inhibitor complex hydrogen bonds in subsites +2, −2, and −3 (Fig. 6). This structure represents the first example in which the +3 binding subsite of HPA has been observed to be occupied by a bound α-1,4–linked glucose unit of an inhibitor. Only limited protein interactions are present in this remote, solvent-exposed surface subsite, which would explain its elusiveness in previous kinetic and structural analyses (Brayer et al. 2000).

Further significant differences are observed in the adjacent chloride ion binding site. In the presence of bound acarbose product, the side chain of D300 is now found

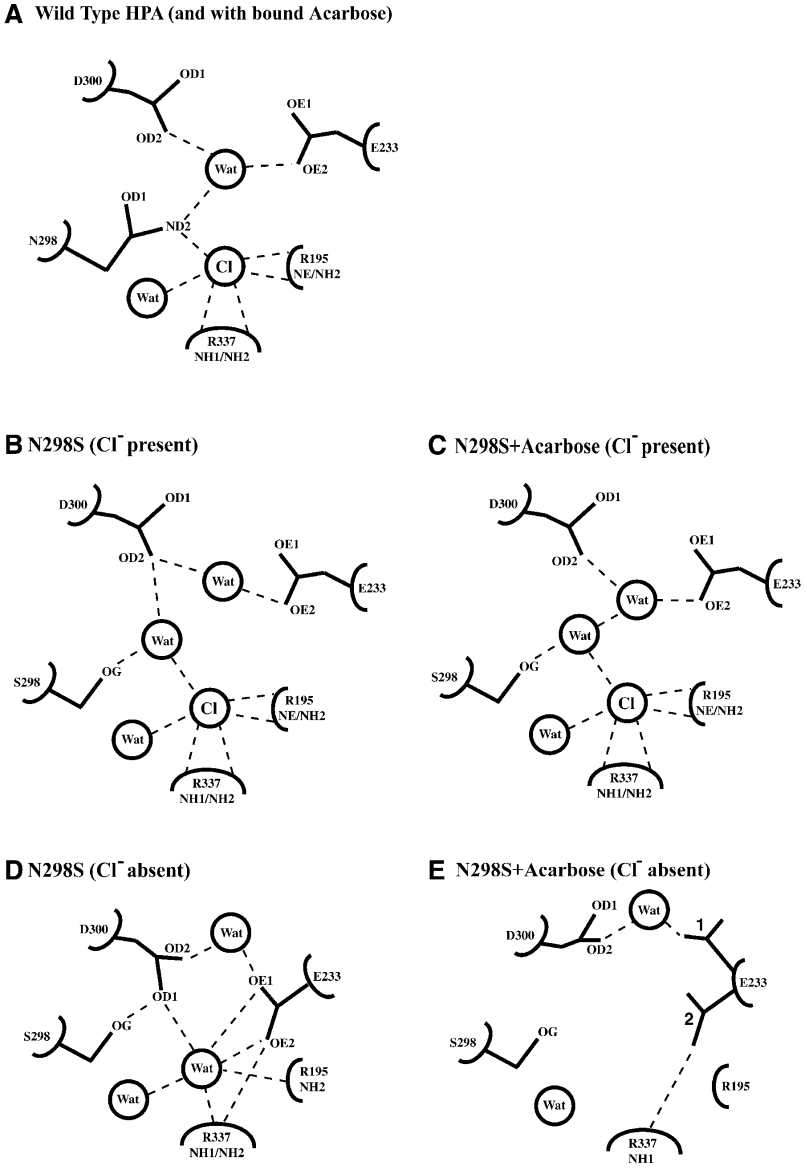

Figure 5. Schematic representations of the hydrogen bond interactions formed within the chloride binding sites in wild-type HPA (and with bound acarbose) (*A*), N298S HPA with bound chloride (*B*), N298S HPA with both bound chloride and acarbose (*C*), N298S HPA in the absence of chloride (*D*), and N298S HPA in the absence of chloride, with acarbose bound (*E*). Note that in the N298S structure without bound chloride, the side chains of D300 and E233 are substantially shifted. For the N298S HPA–acarbose complex (in the absence of chloride), the side chain of E233 takes on two orientations that are approximately equally populated. Here conformation *1* is that found in the wild-type enzyme, while conformation *2* is that observed for the N298S variant without bound chloride and in the absence of acarbose. Bound water molecules are indicated by "Wat" and hydrogen bonds are designated by dashed lines.

oriented in its wild-type conformation, forming two hydrogen bonds to the inhibitor product in the −1 binding subsite (Figs. 5, 6). Surprisingly, the side chain of the acid/base catalyst E233 is found to take on two equally occupied conformations. One of these corresponds to that observed in the absence of bound acarbose product and involves an interaction with the former chloride ion ligand, R337 (Fig. 5). The alternative conformation is that observed in the wild-type HPA/acarbose product complex (Brayer et al. 2000), where the side chain of E233 interacts with inhibitor groups in subsites −1 and +1, about the *N*-linked "glycosidic" bond. It is evident that in the absence of bound chloride ion, the bound acarbose inhibitor product exerts a strong influence on the conformations of residues in the active site. Nonetheless, for E233, this appears insufficient to fully overcome the aberrant interaction of its side chain with the normally unavailable side chain of R337. It seems likely that the unusual product formation observed in this case is a conse-

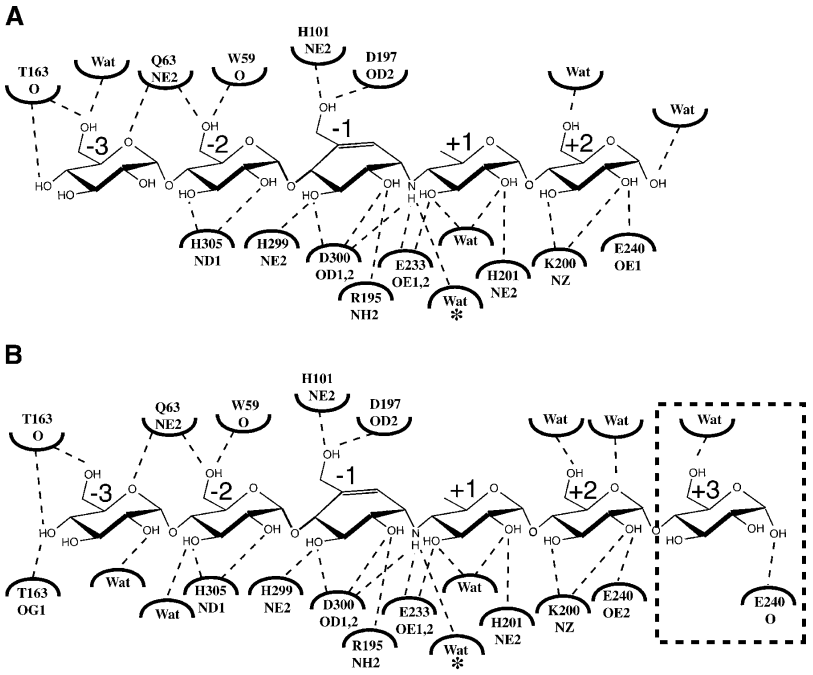

Figure 6. A schematic diagram summarizing the hydrogen bond interactions (dashed lines) to acarbose, when this inhibitor is bound in the active site of the N298S variant of HPA in the presence (*A*) and the absence (*B*) of chloride ion. The normal product of enzymatic inhibitor rearrangement is found in the presence of chloride. Surprisingly, an extended inhibitor product, with an additional glucose unit in binding subsite +3, is found in the absence of chloride (indicated by the dashed box). Active site cleft subsite binding locations have been indicated adjacent to each inhibitor sugar ring. Other prominent hydrogen bonding differences between these complexes occur in subsites −3 and +2. The water molecule believed to play a role in nucleophilic attack on the covalent intermediate generated during hydrolysis of substrates, has been indicated with an *.

quence of E233 not being fully available to the catalytic process. It is also evident that one key role of bound chloride ion is to maintain the wild-type conformation of E233 in both the resting and acarbose-bound enzymes. Notably, the strong influence of bound inhibitor seen in this structure mirrors similar results in the N298S variant structure with bound chloride.

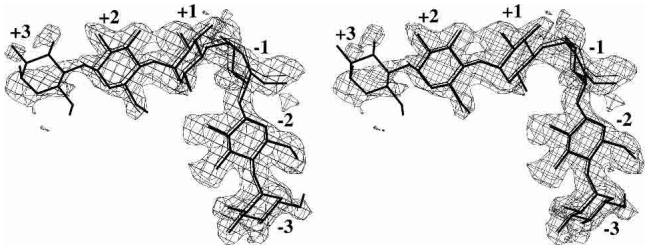

Figure 7. A stereo drawing of the Fo(N298S, chloride absent, acarbose product bound) – Fo(wild-type, chloride present) difference electron density map contoured at the 2σ level. The acarbose product observed for the N298S variant of HPA in the absence of chloride (thick lines), is 1 glucose unit longer (bound in subsite +3) than that observed for the wild-type enzyme (thin lines) or the N298S variant with bound chloride. As can be seen in this map, this extra glucose unit is less tightly bound in the active site of HPA than the remainder of the acarbose inhibitor product.

Mutagenesis studies on TAKA-amylase

Tertiary structural alignment of several chloride-dependent and chloride-independent α-amylases revealed that the spatial positioning of the side chains of R195 and N298 is conserved between the various α-amylases. Somewhat surprising was the fact that the position and orientation of the main chain of R337 is also conserved throughout this family of enzymes, although in chloride-independent α-amylases this residue is not a basic amino acid. It seemed probable that substitution of the nonbasic residue at residue 337, for a basic residue such as arginine, could create a chloride binding site in a previously chloride-independent α-amylase. Furthermore, in the absence of an anion in this space, the newly introduced arginine would provide a positive charge that perturbs the pK_a of the acid/base catalyst in much the same way as has been postulated for the wild-type HPA. In this way a chloride "switch" might be recreated.

Inspection of several chloride-independent α-amylases revealed that the alignment in the region of R337 compared to HPA was best with the α-amylase from the fungus *Aspergillus oryzae* (TAKA-amylase). Comparison of the chloride ion binding site of HPA with the equivalent region of TAKA-amylase reveals a number of amino acid substitutions that likely exclude the possibility of binding chloride

ion at this position in TAKA-amylase. In particular, the chloride ion ligand R337 has been replaced with an isoleucine and the resulting open space is filled by the side chain of W61 (Q41 in HPA) and two water molecules. Further diminishing the volume available are the alternative side chains L250 (T254 in HPA) and to a lesser extent F13 (H15 in HPA). The end result in TAKA-amylase is a rather small internal cavity in this region, which binds a single water molecule. In order to create more space for a chloride ion in this site, therefore, the tryptophan and leucine in this region were also mutated to the corresponding residues in HPA. The final TAKA-amylase variant Ani3038 contained the mutations W61Q, L250T, and I326R (TAKA-amylase numbering).

Kinetic analyses of the wild-type and Ani3038 variant of TAKA-amylase were conducted using CNP-G3 as substrate at both pH 5.0 and 7.0. In standard buffers containing 300 mM chloride, both the wild-type and variant enzymes had similar catalytic activity demonstrating that the triple mutation did not affect the overall catalytic integrity of the enzyme. However, very disappointingly, removal of chloride did not significantly change the activity of the variant, since activities of the Ani3038 and wild-type enzymes were essentially the same at both pH 5.0 and pH 7.0 (Table 1). Therefore the inclusion of chloride in the medium has had no significant effect upon activity for this variant, relative to the wild-type enzyme, or on the pH-dependence, indicating that we were unsuccessful in creating a productive chloride binding site. It would seem that steric electrostatic effects within enzyme active sites are more complex than our straightforward analysis would predict and that even the creation of a simple anion site in a close structural homolog is nontrivial.

Discussion

Structural and mechanistic implications of chloride activation in HPA

Comparison of the kinetic data from wild-type and N298S variant HPA clearly shows that similar trends are seen in both these enzymes at varying chloride concentration. This suggests that while there may be differences in the enzymes, the overall mechanism of chloride activation is retained upon introduction of this mutation to a chloride ion binding site residue. Therefore, the N298S variant HPA should be a good model system for the structural study of chloride activation.

Using the N298S substitution as a model it seems that a major effect of chloride removal is the collapse of several residues into the space thereby generated. Of particular importance are the two catalytic residues E233 (the acid/base catalyst) and D300, which move out of their wild-type positions to interact, either directly or indirectly, with R337. This change in position and environment could easily explain the lower activity and altered pH-dependence observed as chloride concentrations are lowered. The lowering of the pK_a of E233 in the free enzyme (as deduced from the pH-dependence of k_{cat}/K_m for CNP-G3) by 1.5–2 units as chloride concentrations drop (pK_{a2} drops from 7.9 to 6.0) is completely consistent with its coordination to R337. Substrate binding (as reflected by the acarbose-bound data) partially restores the correct interactions, with E233 adopting both positions. Again, this partial restoration is seen in the pH-dependence of k_{cat} using starch as substrate (Numao et al. 2002). In that case, the pK_a of E233 (as reflected in pK_{a2}) dropped from 8.0 to 7.2 upon chloride removal. These findings therefore suggest a relatively simple mechanism for chloride activation of HPA in which binding of chloride both positions E233 and D300 correctly and shields E233 from the positive charge of R337.

Given the simplicity of this mechanism it is perhaps surprising that we were not successful in creating a chloride binding site in TAKA-amylase via the substitutions performed, especially in light of the similarity in structures in the immediate vicinity of the chloride site. This forced us to do a more extensive comparison of the two structures to look for any other factors that had been previously overlooked in this regard. One difference that became apparent was a flexible substrate binding loop in HPA (residues 304–311), which interacts closely with residues involved in the chloride ion binding site but is conspicuously absent in TAKA-amylase. This loop was noted earlier (Brayer et al. 1995) to be more flexible than the rest of the protein (average main chain thermal parameters of 39 $Å^2$) and this flexibility was ascribed to the high glycine content present. Upon binding of substrates or inhibitors this loop reorganizes and rigidifies (thermal parameters of ~24 $Å^2$) with hydrogen bond formation from the side chains of D300 and H305 in the −1 and −2 subsites (Brayer et al. 2000).

This flexible loop is highly conserved in chloride-dependent α-amylases (Table 2), but missing in the chloride-independent enzymes, through both residue deletions and refolding of this region of polypeptide chain away from the active site, facilitated in most cases by the inclusion of a proline in this region. The only apparent exception is the α-amylase of the yellow meal worm (Pereira et al. 1999), which is chloride-dependent but has a shortened substrate binding loop which is folded away from the active site. Of particular significance for this flexible loop are the interactions formed by H305 in the chloride-dependent amylases in the −2 subsite, which are substituted by alternative hydrogen bonds from D340 and R344 in the chloride-independent amylases (TAKA-amylase numbering) (Brzozowski and Davies 1997). These residues are inserted into the active site via the refolding of the loop composed of residues 328–354 in TAKA-amylase. Interestingly these different interactions give rise to a different inhibitor conformation in the −2 and

Table 2. *Flexible substrate binding loop region sequence comparisons between α-amylases of known structure*

PDB code	Organism	Sequence
1. Chloride-dependent α-amylases		
1KB3	Human (pancreatic)	(298) **NHDNQR**GHGAG**G**AS (311)
1C8Q	Human (salivary)	**NHDNQR**GHGAG**G**AS
1BVN	Pig (pancreatic)	**NHDNQR**GHGAG**G**SS
1AQH	*Alteromonas haloplanctis*	**NHDNQR**GHGGA**G**N-
1CLV	Yellow meal worm	**NHDNQR**---TG**G**SQ
2. Chloride-independent α-amylases		
6TAA	*Aspergillus oryzae* (TAKA-amylase)	NH**D**NPR-----FAS
1E3X	*Aspergillus niger*	NH**D**NPR-----FAK
1BLI	*Bacillus licheniformis*	NH**D**TQP-----GQS
1HVX	*Bacillus stearothermophilus*	NH**D**TEP-----GQA
1BAG	*Bacillus subtilis*	SH**D**TYAN----DDE
1AMY	Barley	GT**D**GKAP-------

Protein data bank codes and references for structures cited are: 1KB3, Rydberg et al. (1999); 1C8Q, Ramasubbu et al. (1996); 1BVN, Wiegand et al. (1995); 1AQH, Aghajari et al. (1998); 1CLV, Pereira et al. (1999); 6TAA, Swift et al. (1991); 1E3X, Brzozowski et al. (2000); 1BLI, Machius et al. (1998); 1HVX, Suvd et al. (2001); 1BAG, Fujimoto et al. (1998); 1AMY, Kadziola et al. (1994).

−3 subsites (Fig. 8) as well as a larger rearranged acarbose product, which is reminiscent of the longer, rearranged product seen with the N298S variant in the absence of chloride ion.

The response of this flexible loop to chloride binding in HPA is of interest. In the chloride-free N298S structure S298 swings away to interact with D300, resulting in an altered flexible loop conformation with a poorly organized and shorter helix that ends with a hydrogen bond between the main chain atoms of H299 and Q302. This loop can be restructured to a wild-type conformation either by the binding of chloride or by the binding of substrates, as exemplified by the binding of acarbose. Given the immediate proximity of the catalytically essential residue D300 to this flexible loop, it is then perfectly logical that chloride binding would affect activity in a direct manner. These results suggest that chloride plays a central role in the folding of this flexible loop and thus affects reaction rates, and even products through an additional mechanism.

Taken together, these comparative studies suggest that the chloride-dependent and -independent α-amylases can be thought of as being made up of two rather different active site structural cassettes. The three major components of the chloride-dependent structural unit are the chloride binding site, a helical fold about N298, and an extended flexible substrate binding loop. For the chloride-independent α-amylases, the alternative structural features are a hydrophobic core adjacent to the active site; refolding to provide substitute interactions in the −2 subsite; and reorganization of hydrogen bonding in the N298 region. Given the global similarities of these two types of α-amylases in terms of catalytic mechanism and specificity, it would seem that evolution of these structural alternatives is likely the consequence of optimization for particular operating environments or to produce advantageous product profiles for further metabolism.

Materials and methods

Materials

All buffer salts were obtained from Fisher Scientific Canada. All other chemicals were obtained from Sigma Chemical Co. unless

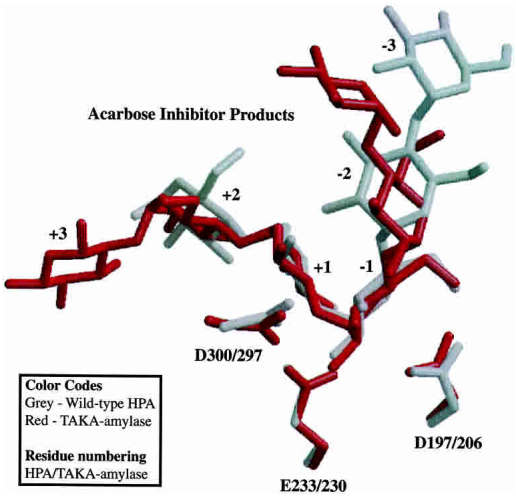

Figure 8. Comparison of the different binding modes of the acarbose inhibitor product in the active sites of the chloride-dependent HPA and the chloride-independent TAKA-amylase (subsites +3 to −3 are labeled). Notably, the end product observed for these two enzymes is also different, with that of TAKA-amylase having an additional glucose in subsite +3. This same inhibitor product is produced in the chloride-deficient N298S variant of HPA (Figure 4).

otherwise noted. 2-Chloro-4-nitrophenyl-α-maltotrioside (CNP-G3) was a kind gift from GelTex Inc.

Bacterial strain, media, and plasmids

Escherichia coli DH5R subcloning efficiency competent cells were obtained from Gibco BRL Products and were used for all transformations and DNA manipulations according to standard procedures (Sambrook et al. 1989). *Pichia pastoris* strain GM5011 was used for the expression of wild-type and variant proteins. Growth and expression media were prepared as published in the *Pichia* expression kit (Invitrogen). The construction of the expression vectors for wild-type HPA (pPIC9-AMY) and the N298S variant of HPA (pPIC9-AMY-N298S) were published previously (Rydberg et al. 1999; Numao et al. 2002).

HPA expression and purification

Transformation of HPA plasmids into *P. pastoris* cells and subsequent selection was carried out according to directions in the *Pichia* expression kit (Invitrogen) and as described previously (Rydberg et al. 1999; Numao et al. 2002). Enzyme concentrations were determined spectrophotometrically by using $A^{0.1\%} = 2.2$ at 280 nm for both wild-type and N298S variant HPAs.

TAKA-amylase variant preparation

The expression vector used in the study of TAKA-amylase (pTOC53) was created by cutting the gene out of pTAKA17 (Christensen et al. 1988) using EcoR1 and introducing it into pUC19, cut with the same restriction enzyme. Introduction of the substitutions W61Q, L250T, and I326R into this expression vector was accomplished using the QuikChange Multi Site directed mutagenesis kit (Stratagene, cat. no. 200513) according to the instructions provided by the manufacturer. The phosphorylated primers used for mutagenesis were as follows: tcacagccatccagatcaccccg (W61Q), tggacggcgtaacgaactcccatttactat (L250T), and gacggaatccccatctac gccg (I326R). Confirmation of the presence of these substitutions and the absence of any other secondary mutations was accomplished by sequencing of the gene.

The resulting variant plasmid (Ani3038) was transformed into *Aspergillus orzyae*, and this strain was shown to express the recombinant protein. This strain was then inoculated in G2-gly media (yeast extract (Difco 0127 109-0569) 18 g/L, glycerol 87% (Merck 4094) 24 g/L, pluronic PE-6100 (BASF 102-3098) 1 mL/L), and grown overnight at 34°C, after which 2 mL of this solution was transferred to 100 mL 2×MDU media (maltose 45 g/L, $MgSO_4 \cdot 7H_2O$ 1 g/L, NaCl 1 g/L, K_2SO_4 2 g/L, KH_2PO_4 12 g/L, yeast extract (Difco 212750109) 0.5697 g/L, pluronic PE 6100 (BASF 102-30980) 1 mL/L, $ZnCl_2$ 6.8 g/L, $CuSO_4 \cdot 5H_2O$ 2.5g/L, $NiCl_2 \cdot 6H_2O$ 0.24 g/L, $FeSO_4 \cdot 7H_2O$ 13.9 g/L, $MnSO_4 \cdot H_2O$ 8.45 g/L, citric acid 3 g/L, maltose sirup (~75%) 160 g/L), and the culture was further grown for 3 d at 34°C. The fermentation broth was then filtered, and the protein precipitated with 3 M ammonium sulphate followed by centrifugation at 10,000*g*. The resultant pellet was dissolved in water and dialyzed against 10 mM sodium acetate buffer (pH 5.2), and then loaded onto a Q-Sepharose (HiLoad 26/10, Pharmacia) column. The protein was eluted with a linear salt gradient from 10 to 250 mM sodium acetate buffer (pH 5.2), and the fractions containing amylase activity were pooled and stored at −20°C. The concentration of the purified sample was determined by amino acid analysis using a Biochrom 20 plus amino acid analyzer.

Kinetic analyses

Standard assays for the wild-type and N298S variant HPAs were carried out at 30°C in 20 mM sodium phosphate buffer (pH 7.0), using 2.0 mM CNP-G3 as substrate. Hydrolysis of CNP-G3 was followed by measurement of the increase in absorbance at 400 nm using a Varian CARY 4000 spectrophotometer attached to a temperature control unit. The pH dependence of wild-type and variant HPA activities was determined by varying the pH of the sodium phosphate buffer from pH 4.0 to 10.0. Plots of pH versus activity were fit to a double ionization pH curve by nonlinear regression assuming k_{cat}/K_m values of 0 at pH extremes and the pH-independent k_{cat}/K_m values in the mid-range indicated in the table, using the program GraFit 4.0.21 (R.J. Leatherbarrow, Erithacus Software Ltd.). The dependence of wild-type and variant HPA activities on chloride concentration at different pH values was determined by varying chloride concentrations from 0.25 mM to 10 mM for wild-type and 10 mM to 600 mM for N298S HPA. The data (chloride concentration vs. activity) were fit to a ligand binding equation by nonlinear regression using the program GraFit 4.0.21. Using CNP-G3 as substrate, the kinetic parameters for k_{cat}, K_m, and k_{cat}/K_m were determined by fitting the data to the Michaelis-Menten equation using nonlinear regression with the program GraFit 4.0.21. Substrate concentrations were varied from $0.3 \times K_m$ to $5 \times K_m$. The same standard assays were used to measure kinetic values for TAKA-amylase and its Ani3038 variant. To study the effect of pH, measurements were made at pH 5.0 and 7.0, and with chloride concentrations of 0 and 300 mM. Additional experiments were also conducted at pH 7.0 on both the wild-type and variant TAKA-amylase, in which the chloride concentration was varied in finer increments. A compilation of kinetic values obtained for the HPA and TAKA-amylase enzymes is presented in Table 1.

Structure determinations

Crystals of the N298S variant of HPA were grown in the absence of chloride ion, but otherwise using conditions previously described for the wild-type enzyme (Brayer et al. 2000). Variant crystals with bound chloride were prepared by soaking crystals in a solution containing 300 mM NaCl for 30 min. Acarbose-complexed variant crystals were prepared for structural analysis by soaking in a solution containing 200 mM acarbose for 30 min.

Diffraction data for all crystals were collected on a Mar345 imaging plate area detector system at 298 K using Cu Kα radiation supplied by a Rigaku RU300 rotating anode generator operating at 50 kV and 100 mA. Intensity data were integrated, scaled, and reduced to structure factor amplitudes, with the HKL suite of programs (Otwinowski and Minor 1997).

Crystals of N298S variant HPA, in the absence and presence of either chloride ion or acarbose, were isomorphous with those of wild-type HPA (Brayer et al. 1995) and as such, this latter structure was used as the starting refinement model for all structure determinations (with residue 298 initially represented as an alanine). Structural refinements were carried out with the CNS software program (Brunger et al. 1998). In these analyses, cycles of positional, and thermal B refinements, were alternated with manual model rebuilding with O (Jones et al. 1991). In the initial stages of this process, the complete polypeptide chain of each refinement model was adjusted based on omit maps (with ~20

Table 3. *Summary of data collection and structure determination statistics*

Structure determination	N298S (no Cl^-)	N298S +Cl^-	N298S +Acarbose (no Cl^-)	N298S +Acarbose +Cl^-
Data collection				
Space group	$P2_12_12_1$	$P2_12_12_1$	$P2_12_12_1$	$P2_12_12_1$
Unit cell dimensions (Å)				
a	53.3	53.0	53.4	53.1
b	69.0	69.3	69.1	69.4
c	132.1	132.1	132.4	132.4
Number of unique reflections	33,697	32,178	33,885	25,669
Mean $I/\sigma I$[a]	16.4 (4.4)	22.4 (13.6)	17.2 (4.4)	16.7 (4.9)
Multiplicity[a]	4.1 (4.0)	5.1 (4.7)	4.9 (4.6)	4.2 (3.3)
Merging *R*-factor (%)[a]	5.5 (21.5)	3.9 (11.5)	8.6 (25.6)	8.0 (20.2)
Maximum resolution (Å)	2.00	2.03	2.00	2.20
Structure refinement				
Number of reflections	32,797	31,953	33,006	25,038
Resolution range (Å)	10–2.00	10–2.03	10–2.00	10–2.20
Completeness within range (%)[a]	93 (89)	99 (99)	98 (93)	97 (87)
Number of protein atoms	3943	3943	3943	3943
Number of water molecules	332	343	279	315
Number of inhibitor atoms	—	—	57	57
Average thermal factors ($Å^2$)				
Protein atoms	22.1	23.9	21.4	28.1
Chloride ion	—	21.9	—	19.9
Acarbose ligand	—	—	37.0	66.1
Water molecules	44.4	44.7	41.4	45.9
Final *R*-factor/*R*-free (%)[b]	15.5/20.0	16.3/20.7	16.4/20.5	15.6/21.4
Structure stereochemistry		r.m.s. deviations		
Bonds (Å)	0.006	0.007	0.003	0.007
Angles (°)	1.6	1.1	1.3	1.1

[a] Values in parentheses refer to the highest resolution shell: 2.07–2.00 Å for the N298S (no Cl^-) and N298S + Acarbose (no Cl^-) structures; 2.03–2.08 Å for the N298S + Cl^- structure; and 2.24–2.20 Å for the N298S + Acarbose + Cl^- structure determination.
[b] For the *R*-free test, 5% of the diffraction data were kept aside.

residues omitted in each). It was at this stage that the side chain of the serine at position 298 was placed based on observed electron density. Subsequently, the complete polypeptide chain was examined periodically with F_o–F_c and $2F_o$–F_c difference electron density maps. Following refinement of the N298S variant polypeptide chain, bound chloride, and/or acarbose in complexed structures were positioned on the basis of F_o–F_c difference electron density maps. For such complexes, all atoms were then jointly refined to obtain the best overall fit. Both chloride and acarbose were found to be well resolved in electron density maps and to bind at full occupancy in these complexes, with thermal factors comparable to the surrounding protein structure. In addition, the *N*-acetylglucosamine moiety bound to the side chain of N461 in all N298S variant structures was refined accordingly. At this point, solvent molecules were identified from a further F_o–F_c difference electron density map and included in the refinement model based on hydrogen bonding potential to protein atoms and the refinement of a thermal factor of <75 $Å^2$. In a final phase, protein, chloride, inhibitor, and solvent molecules were jointly refined to convergence. The final data collection and refinement statistics obtained are detailed in Table 3. Atomic coordinates and structure factors arising from structure determinations have been deposited in the Protein Data Bank, Research Collaboratory for Structural Bioinformatics, Rutgers University, New Brunswick, NJ (http://www.rcsb.org/).

Acknowledgments

This work was supported by an operating grant from the Canadian Institutes of Health Research (CIHR). We thank Dr. D.G. Kilburn for the generous gift of the endoglycosidase F-cellulose binding domain fusion protein. Figures 1, 4, and 8 were prepared with the assistance of Molscript (Kraulis 1991) and Raster3D (Merritt and Bacon 1997). Figures 3 and 7 were prepared with the assistance of X-PLOR (Brunger 1996) and SETOR (Evans 1993).

References

Aghajari, N., Feller, G., Gerday, C., and Haser, R. 1998. Crystal structures of the psychrophilic α-amylase from *Alteromonas haloplanctis* in its native form and complexed with an inhibitor. *Protein Sci.* **7:** 564–572.

———. 2002. Structural basis of α-amylase activation by chloride. *Protein Sci.* **11:** 1435–1441.

Boel, E.L., Brady, A.M., Brzozowski, Z., Derewenda, G.G., Dodson, V.J., Jensen, S.B., Petersen, H., Swift, L., Thim, L., and Woldike, H.F. 1990. Calcium binding in α-amylases: An X-ray diffraction study at 2.1-Å resolution of two enzymes from *Aspergillus*. *Biochemistry* **29:** 6244–6249.

Braun, C., Brayer, G.D., and Withers, S.G. 1995. Mechanism-based inhibition of yeast α-glucosidase and human pancreatic α-amylase by a new class of inhibitors: 2-Deoxy-2,2-difluoro α-glycosides. *J. Biol. Chem.* **270:** 26778–26781.

Brayer, G.D., Luo, Y.G., and Withers, S.G. 1995. The structure of human

pancreatic α-amylase at 1.8 Å resolution and comparisons with related enzymes. *Protein Sci.* **4:** 1730–1742.

Brayer, G.D., Sidhu, G., Maurus, R., Rydberg, E., Braun, C., Wang, Y., Nguyen, N., Overall, C., and Withers, S. 2000. Subsite mapping of the human pancreatic α-amylase active site through structural, kinetic and mutagenesis techniques. *Biochemistry* **39:** 4778–4791.

Brunger, A.T. 1996. *X-PLOR version 3.8*. Yale University Press, New Haven, CT.

Brunger, A.T., Adams, P.D., Clore, G.M., DeLano, W.L., Gros, P., Grosse-Kunstleve, R.W., Jiang, J.-S., Kuszewski, J., Nilges, M., Pannu, N.S., et al. 1998. Crystallography & NMR system: A new software suite for macromolecular structure determination. *Acta Crystallogr. D* **54:** 905–921.

Brzozowski, A.M. and Davies, G.J. 1997. Structure of the *Aspergillus oryzae* α-amylase complexed with the inhibitor acarbose at 2.0 Å resolution. *Biochemistry* **36:** 10837–10845.

Brzozowski, A.M., Lawson, D.M., Turkenburg, J.P., Bisgaard-Frantzen, H., Svendsen, A., Borchert, T.V., Dauter, Z., Wilson, K.S., and Davies, G.J. 2000. Structural analysis of a chimeric bacterial α-amylase. High resolution analysis of native and ligand complexes. *Biochemistry* **39:** 9099–9107.

Christensen, T., Woeldike, H., Boel, E., Mortensen, S.B., Hjortshoej, K., Thim, L., and Hansen, M.T. 1988. High level expression of recombinant genes in *Aspergillus oryzae*. *Bio/Technology* **6:** 1419–1422.

D'Amico, S., Gerday, C., and Feller, G. 2000. Structural similarities and evolutionary relationships in chloride-dependent α-amylases. *Gene* **253:** 95–105.

Evans, S.V. 1993. SETOR: Hardware lighted three-dimensional solid model representations of macromolecules. *J. Mol. Graph.* **11:** 134–138.

Feller, G., Bussy, O., Houssier, C., and C. Gerday, G. 1996. Structural and functional aspects of chloride binding to *Alteromonas haloplanctis* α-amylase. *J. Biol. Chem.* **271:** 23836–23841.

Fujimoto, Z., Takase, K., Doui, N., Momma, M., Matsumoto, T., and Mizuno, H. 1998. Crystal structure of a catalytic-site mutant α-amylase from *Bacillus subtilis* complexed with maltopentaose. *J. Mol. Biol.* **277:** 393–407.

Jones, T.A., Zhou, J.-Y., Cowan, S.W., and Kjeldgaard, M. 1991. Improved methods for building protein models in electron density maps and the location of errors in these models. *Acta Crystallogr. A* **47:** 110–119.

Kadziola, A., Abe, J., Svensson, B., and Haser, R. 1994. Crystal and molecular structure of barley α-amylase. *J. Mol. Biol.* **239:** 104–121.

Kraulis, P.J. 1991. MOLSCRIPT: A program to produce both detailed and schematic plots of protein structures. *J. Appl. Crystallogr.* **24:** 946–950.

Levitzki, A. and Steer, M.L. 1974. The allosteric activation of mammalian α-amylase by chloride. *Eur. J. Biochem.* **41:** 171–180.

Machius, M., Wiegand, G., and Huber, R. 1995. Crystal structure of calcium-depleted *Bacillus licheniformis* α-amylase at 2.2 Å resolution. *J. Mol. Biol.* **246:** 545–559.

Machius, M., Declerck, N., Huber, R., and Wiegand, G. 1998. Activation of *Bacillus licheniformis* α-amylase through a disorder→order transition of the substrate-binding site mediated by a calcium–sodium–calcium metal triad. *Structure* **6:** 281–292.

Merritt, E.A. and Bacon, D.J. 1997. Raster3D photorealistic molecular graphics. *Methods Enzymol.* **277:** 505–524.

Numao, S., Maurus, R., Sidhu, G., Wang, Y., Overall, C.M., Brayer, G.D., and Withers, S.G. 2002. Probing the role of the chloride ion in the mechanism of human pancreatic α-amylase. *Biochemistry* **41:** 215–225.

Otwinowski, Z. and Minor, W. 1997. Processing of X-ray diffraction data collected in oscillation mode. *Methods Enzymol.* **276:** 307–326.

Pereira, P.J.B., Lozanov, V., Patthy, A., Huber, R., Bode, W., Pongor, S., and Strobl, S. 1999. Specific inhibition of insect α-amylases: Yellow meal worm α-amylase in complex with the amaranth α-amylase inhibitor at 2.0 Å resolution. *Structure* **7:** 1079–1088.

Ramasubbu, N., Paloth, V., Luo, Y.G., Brayer, G.D., and Levine, M.J. 1996. Structure of human salivary α-amylase at 1.6-Å resolution—Implications for its role in the oral cavity. *Acta Crystallogr. D Biol. Crystallogr.* **52:** 435–446.

Rydberg, E.H., Sidhu, G., Vo, H.C., Hewitt, J., Cote, H.C., Wang, Y., Numao, S., MacGillivray, R.T., Overall, C.M., Brayer, G.D., et al. 1999. Cloning, mutagenesis, and structural analysis of human pancreatic α-amylase expressed in *Pichia pastoris*. *Protein Sci.* **8:** 635–643.

Rydberg, E.H., Li, C., Maurus, R., Overall, C.M., Brayer, G.D., and Withers, S.G. 2002. Mechanistic analyses of catalysis in human pancreatic α-amylase: Detailed kinetic and structural studies of mutants of three conserved carboxylic acids. *Biochemistry* **41:** 4492–4502.

Sambrook, J., Fritsch, E.F., and Maniatis, T. 1989. *Molecular cloning: A laboratory manual*. Cold Spring Harbor Laboratory, Cold Spring Harbor, NY.

Steer, M.L. and Levitzki, A. 1973. The metal specificity of mammalian-amylase as revealed by enzyme activity and structural probes. *FEBS Lett.* **31:** 89–92.

Suvd, D., Fujimoto, Z., Takase, K., Matsumura, M., and Mizuno, H. 2001. Crystal structure of *Bacillus stearothermophilus* α-amylase: Possible factors determining the thermostability. *J. Biol. Chem.* **129:** 461–468.

Swift, H.J., Brady, L., Derewenda, Z.S., Dodson, E.J., Dodson, G.G., Turkenburg, J.P., and Wilkinson, A.J. 1991. Structure and molecular model refinement of *Aspergillus oryzae* (TAKA) α-amylase: An application of the simulated-annealing method. *Acta Crystallogr. B* **47:** 535–544.

Tao, B.Y., Reilly, P.J., and Robyt, J.F. 1989. Detection of a covalent intermediate in the mechanism of action of porcine pancreatic α-amylase by using 13C nuclear magnetic resonance. *Biochim. Biophys. Acta* **995:** 214–220.

Uitdehaag, J.C., Mosi, R., Kalk, K.H., van der Veen, B.A., Dijkhuizen, L., Withers, S.G., and Dijkstra, B.W. 1999. X-ray structures along the reaction pathway of cyclodextrin glycosyltransferase elucidate catalysis in the α-amylase family. *Nat. Struct. Biol.* **6:** 432–436.

Vasella, A., Davies, G.J., and Bohm, M. 2002. Glycosidase mechanisms. *Curr. Opin. Chem. Biol.* **6:** 619–629.

Wakim, J., Robinson, M., and Thoma, J.A. 1969. The active site of porcine-pancreatic α-amylase: Factors contributing to catalysis. *Carbohydr. Res.* **10:** 487–503.

Wiegand, G., Epp, O., and Huber, R. 1995. The crystal structure of porcine pancreatic α-amylase in complex with the microbial inhibitor Tendamistat. *J. Mol. Biol.* **247:** 99–110.

Zechel, D.L. and Withers, S.G. 2000. Glycosidase mechanisms: Anatomy of a finely tuned catalyst. *Acc. Chem. Res.* **33:** 11–18.